Chapter 5

Pd@TTF Tailored Nanostructured Platform: Voltammetric Estimation of Ceftazidime

5.1 Introduction

Ceftazidime (CFZ) is a semi synthetic and one of the third generation vaccines of β-lactam family. It is a broad-spectrum antibiotic active against several gram positive and gram-negative bacterial strains and comes under the category of cephalosporin. Due to its antibacterial activity and pharmacokinetic properties, [Gringauz *et al.*, 1997; Garzone *et al.*, 1983; Reeves *et al.*, 1980; Kamimura *et al.*, 1979] it is a potent agent used against *Pseudomonas aeruginosa* infections. CFZ is widely used for the treatment of patients infected with respiratory tract infections viz. pneumonia, soft tissue infections, bone infections, abdominal infections and lung infections in patients suffering from cystic fibrosis and urinary tract related infections [Rahway *et al.*, 1983; Florey *et al.*, 1990]. Although CFZ is one of the vaccine of the choice of interest for bacterial infections, it has also exhibited an excellent record of clinical success; strict control of its dosage is required since its high dosage in infected patients can cause various side effects such as renal tubular necrosis [Barza *et al.*, 1978]. This drug is potentially nephrotoxic when administered in high dosage. This is the reason why its determination is crucial in humans. Various techniques such as High performance liquid chromatography (HPLC) [Hwang *et al.*, 1984; Leeder *et al.*, 1983; Ayrton *et al*;1981; Myers *et al.*,1983; Tyczkowska *et al*; 1992 *et al.*, Nahata *et al.*, 1992], colorimetry, microbiological etc. have been extensively used for the determination of CFZ [Thornton *et al.*,1981; El-Maali *et al.*,2000; Ferreira *et al.*,1997; Ferreira *et al.*, 1997; El-Maali *et al.*, 1991, Ogorevc *et al.*, 1991; Kim *et al.*, 1991]. These conventional sensing methods are highly sophisticated, time consuming and less sensitive. In comparison to other

methods, electrochemical method is more superior because it is very simple, sensitive and less time consuming. Reviewing the literature it reveals that a few reports are available related to its detection using voltammetric methods on modified solid-state electrodes. However, there is a need to develop more reliable and sensitive technique for the quick detection of drug molecules. Third generation antibiotics like CFZ can be given to HIV-1 patients frequently as HIV-1 patients can easily suffer from opportunistic infections i.e. they are more prone to bacterial infections due to their weak immune systems. Therefore, detection of this drug is very crucial for the patients suffering from HIV-1.

Immense attentions have been drawn by researchers towards the application of noble metal nanostructures (NMN) in various fields such as sensors, nano electronic, optics, biochemical and catalysis [Wang *et al.*, 2002; Pethkar *et al.*, 2001; Gupta *et al.*, 2015; Baby *et al.*, 2011; Aragay *et al.*, 2012; Shi *et al.*, 2016]. Catalytic efficiency of nanomaterials is significantly affected by their shape and size [Ahmadi *et al.*, 1995; Fendler *et al.*, 1996]. Recently, researchers have depicted keen interests in nanomaterials due to their supramolecular chemistry, which helps in significant enhancement of properties and further performance of devices [Sharma *et al.*, 1995]. Incorporation of noble metals with other inexpensive and sustainable organic/biomaterials is believed as one of the most fascinating ways to modify their properties. Incorporation of NMN have been successfully performed in various biomaterials, polymers, organic molecules, and carbon materials, showing their potential applications in diverse fields [Lopes *et al.*, 2001; Konnova *et al.*, 2015; Gupta *et al.*, 2014; Pandey *et al.*, 2012; Shahrokhian *et al.*, 2012]. The most facile method of metal organic complex formation or metal nanoparticles stabilization with organics is coordination with π electron donor organic molecules.

Tetrathiafulvalene (TTF), sulphur containing non-aromatic compound having 14π electron system and showing prominent redox properties, is one of the most versatile molecule. On oxidation, TTF forms a radical cation, which is stable and known to exist as a paramagnetic species at room temperature. Oxidised TTF species have a high tendency to form dimers or higher aggregates. Oligomeric TTF derivatives such as dendrimer (dication) exhibit a broad band at 800 nm due to intra and inter molecular π-π* interaction in between TTF radical cations [Adam *et al.*, 1994; Jogerson *et al.*, 1994; Bryce *et al.*, 1995]. TTF has been proved as an excellent π electron donor due to its tendency to easily form the radical cation and dication products which protect metal nanoparticles from aggregation and can be used as a stabilising agent because they tend to self-assemble through π-π* and S-S interactions into nanostructures [Canvert *et al.*, 2015]. Metal-TTF interaction has been reported earlier by Xiaqin *et al.* in which silver dendritic nanostructure was stabilised by TTF in acetonitrile [Wang *et al.*, 2003]. Nakai *et al.* also studied electro active TTF-Au nanocomposite and their stable film on Au electrode [Nakai *et al.*, 1999]. Christian *et al.* reported the synthesis and electrochemistry of a TTF glycol dendrimer and its aggregation [Christensen *et al.*, 1998].

Herein, we have adopted a very simple chemical method for the synthesis of TTF stabilised Pd^0 NPs and their subsequent application for detection of an important drug CFZ, using a very simple electrochemical technique. We have compared the analytical performance of the prepared catalyst with previously prepared catalysts used for CFZ determination.

5.2 Experimental

5.2.1 Materials

Tetrathiafulvalene and $PdCl_2$ were received from Sigma Aldrich, U.S.A. Ceftazidime (CFZ) pentahydrate; Na_2HPO_4, NaH_2PO_4, deionised water, ethanol and KCl were procured either from SRL or Merck, India. All chemicals utilized were of analytical grade and used as received without further purification. All the experiments were performed at room temperature (25±2 ºC). Prior to electrochemical measurement solution was purged with high purity N_2 gas for 15-20 min.

5.2.2 Synthesis of TTF stabilized Pd Nanoparticles (Pd@TTF)

Palladium and TTF composites (Pd@TTF) in one pot synthesis were prepared by very simple procedure, initially 7.5 mg of TTF in 2 mL of ethanol and stirred in ice bath for 30 minutes. In another vessel, 10 mM of $PdCl_2$ was dissolved in acidified distilled water. After that, $PdCl_2$ solution was drop-wise added to TTF solution and colour of TTF solution was gradually changed to dark bluish green. Prepared composite is denoted as Pd@TTF. As prepared composite was washed several time with Mill-Q water and ethanol mixture and centrifuged at 6000 rpm to remove unreacted excess materials. The resultant colloidal solution was further used for optical/electrochemical measurement and characterization. Figure 5.1 shows the schematic pathways for the preparation of Pd@TTF composite. The prepared Pd@TTF rinsed several times with Milli Q water and ethanol to get rid of any unreacted impurities. As-prepared resulting solution was centrifuged at 6000 rpm to receive the content of nano Pd protected with TTF for 10 minutes and decanted. Then, resultant colloidal suspension was kept for

characterisation and further experimentation. Figure 5.1 describes the synthesis of Pd@TTF using two simple accessible components in a single step.

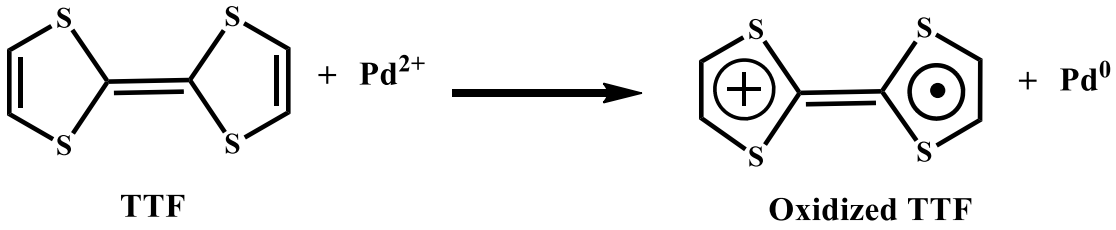

Figure 5.1 Schematic showing **s**ynthesis of Pd@TTF using two simple accessible components in a single step.

5.2.3 Instrumentation

The electrochemical experiments were performed with a CHI-7041C (CH Instruments, USA), using three-electrode system with GC (CH Instruments, area =0.07 cm^2) or modified GC as working electrode, Pt disk (3.3mm) as counter electrode and Ag/AgCl (saturated with KCl) as reference electrode. UV-Vis. absorption spectral changes were recorded with Lambda-25 Perkin Elmer Spectrophotometer, Germany. Fourier transforms infrared (FT-IR) measurement were executed using Nicolet-6700 U.S.A. Nanocrystals structure of palladium was analysed using Transmission electron microscopy with HRTEM Tecnai G^2 20 S-Twin FEI Corporation, Netherlands operating at 200KV by taking a few µL of colloidal palladium suspension on carbon coated copper grid. X-ray photoelectron spectrum (XPS) was recorded for elemental analysis using Kratos Analytical instrument, Shimadzu group company Amicus XPS, UK.

5.2.4 Preparation of Modified Electrode

The glassy carbon (GC) electrode with geometrical diameter of 3.0 mm was employed for the modification of Pd@TTF nanostructures. Prior to the modification, GC electrode

was cleaned with 0.05µm alumina slurry on a wet polishing pad and washed several times with double distilled water. After that, it was sonicated in water for 2 minutes. The colloids of as-prepared Pd@TTF nanostructures were drop casted over the GC electrode surface and allowed to dry at room temperature for 6-8 h and then used for electrochemical measurements.

5.3 Results and discussion

5.3.1 Spectroscopic Characterization of Prepared Composite

Figure 5.2 (A) shows the UV-visible spectra of TTF in which strong and weak absorption peaks were observed at 309 and 368 nm which correspond to π-π* and n-π* transitions respectively. Composite material (Pd@TTF) exhibits major absorption peaks in the visible region corresponding to π-π* transition at 437 nm and 584 nm respectively, which can be attributed to the formation of TTF radical cations [Torrance *et al.*, 1979]. The absorption peak obtained at 309 nm is due to unreacted TTF in the reaction content. During the reaction, TTF is oxidised to TTF radical cation and palladium is reduced (Pd^{2+} to Pd^{0}). Further, agglomeration of Pd NPs was protected due to the presence of oxidised product of TTF and its radical cation. These oxidised products also help in capping the palladium nanostructures and further provide the stability to palladium nanostructures through interaction with sulphur moieties.

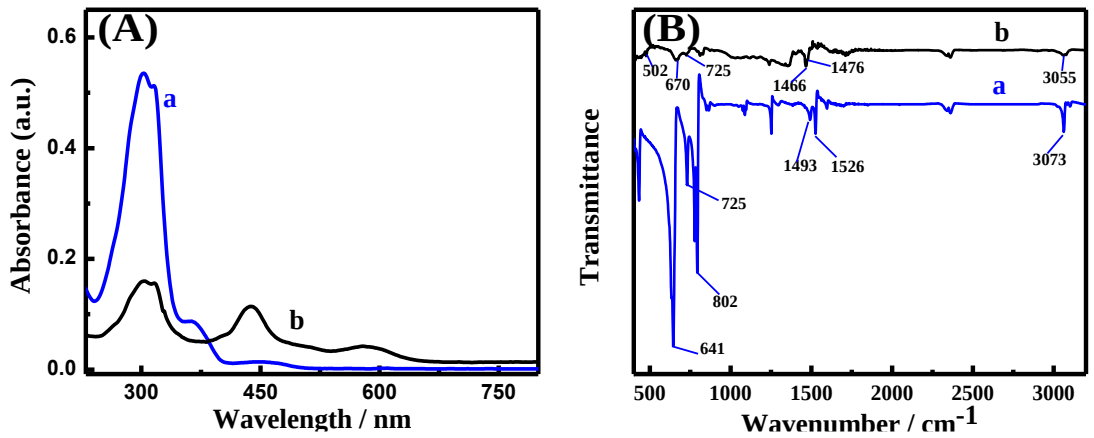

Figure 5.2 (A) UV-vis. absorption spectra of (a**)** TTF (b**)** Pd@TTF. (B) FT-IR spectra of (a) TTF and (b**)** Pd@TTF.

FT-IR spectroscopy was also used to characterize and see the probable interactions between TTF and Pd. Figure 5.2 (B) shows the FT-IR spectra of TTF (a) and Pd@TTF (b). Characteristics absorption frequencies were assigned from the literature corresponding to various functional groups present in its structure. In case of TTF, -C-H stretching, -C=C asymmetric, anti-symmetric stretching and -C-S stretching vibrations were observed at 3073, 1493, 1526 and 641 cm^{-1} respectively. The bands observed at 802 $cm^{-1}$and 725 cm^{-1} can be attributed to -C=C-H out of plane vibration [Bozio *et al.*, 1979; Bozio *et al.*, 1977] In case of Pd@TTF, same peaks were observed at 3055, 1466, 1476 cm^{-1} respectively. Out of plane vibrations of -C=C-H were also shifted to 670 and 725 cm^{-1}. As, it can be seen from the FT-IR spectra of Pd@TTF all the vibrations were shifted towards lower wavenumbers, which could be due to interaction of TTF with Pd. A noticeable decrease in the -S-H stretching frequency was observed, which was shifted from 641 to 502 cm^{-1}. This much large shift in vibration frequency could be strong electrostatic interaction between Pd and S and transfer of electron density from sulphur to Pd. This interaction was further confirmed by XPS.

5.3.2 Microscopic Characterisation and Elemental Analysis

Figure 5.3 (a) shows the TEM image of Pd@TTF composite, in which spherical Pd NPs are dispersed in the TTF matrix. The average diameter of as-prepared Pd nanoparticles was found to be 30-40 nm. Figure 5.3(b) shows the selected area electron diffraction (SAED) pattern of palladium NPs. From SAED pattern it is clear that Pd@TTF shows crystalline behaviour and the Scherrers ring of Pd NPs corresponds to (200), (220), (111), (311) planes of face centre cubic lattice. EDX measurement was also executed to examine the elemental composition of Pd@TTF (Figure 5.3c).

It indicates the presence of carbon, sulphur and palladium atom and confirms that the Pd@TTF consist predominantly Pd and S. X-ray photoelectron spectroscopy (XPS) was carried out to get some idea about the oxidation state and chemical environment of other atoms in composite material (Pd@TTF). XPS spectrum of Pd exhibits two peaks at 335.5 eV and 340.6 eV corresponding to Pd $^{3}d_{5/2}$ and Pd $^{3}d_{3/2}$ oxidation states respectively. These values of binding energies are in good agreement with zero oxidation sates of Pd. For sulphur, one XPS peak was observed at 162.5 eV which corresponds to $S^{2}p_{3/2}$ state, which is very similar to the sulphur atom attached to gold nanoparticles reported by Gobbo et al [Gobbo *et al.*, 2013].

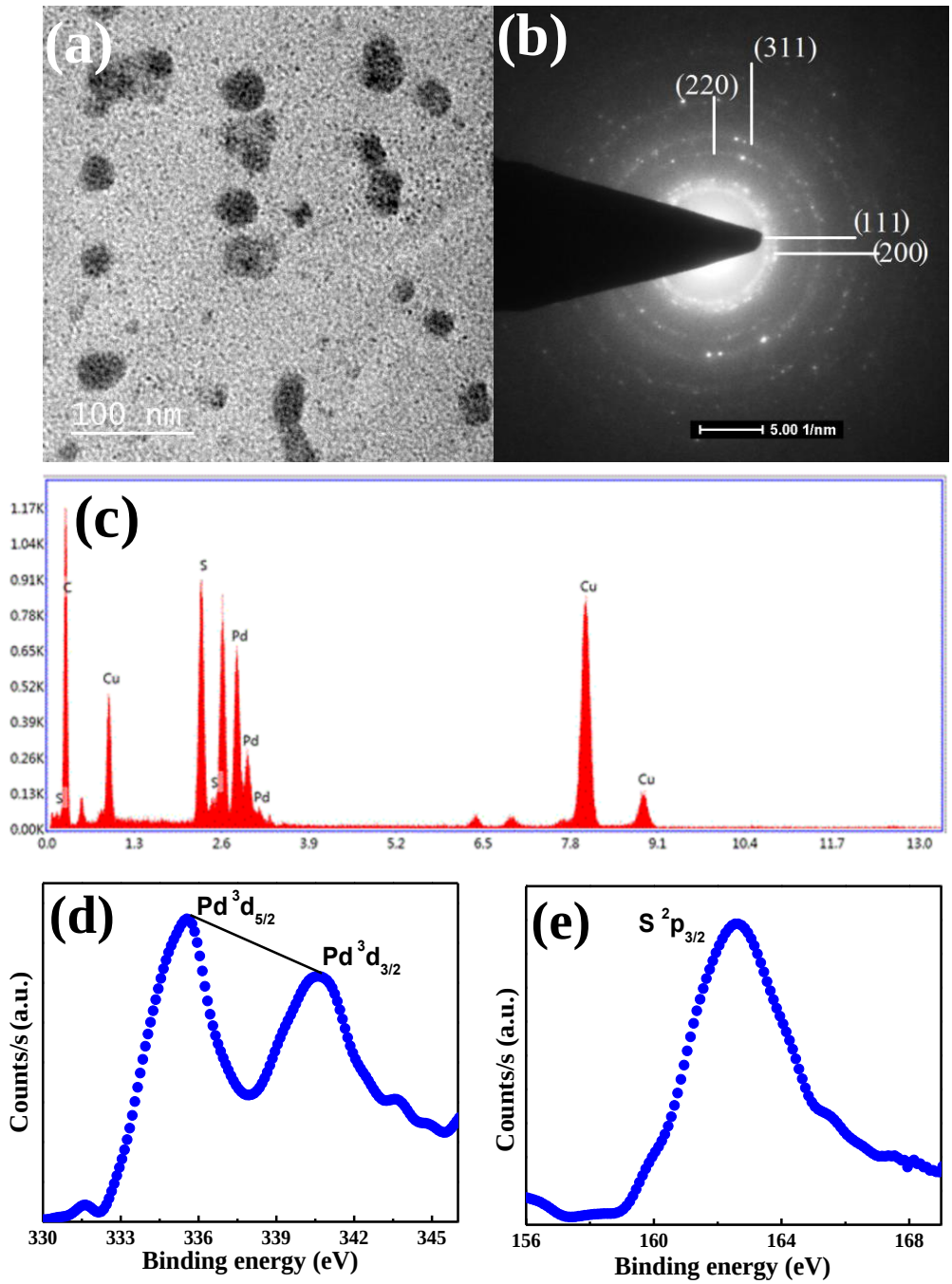

Figure 5.3 TEM image of Pd@TTF (a), SAED pattern (b) and EDAX pattern (c), deconvoluted peak for Pd (d) and sulphur (e).

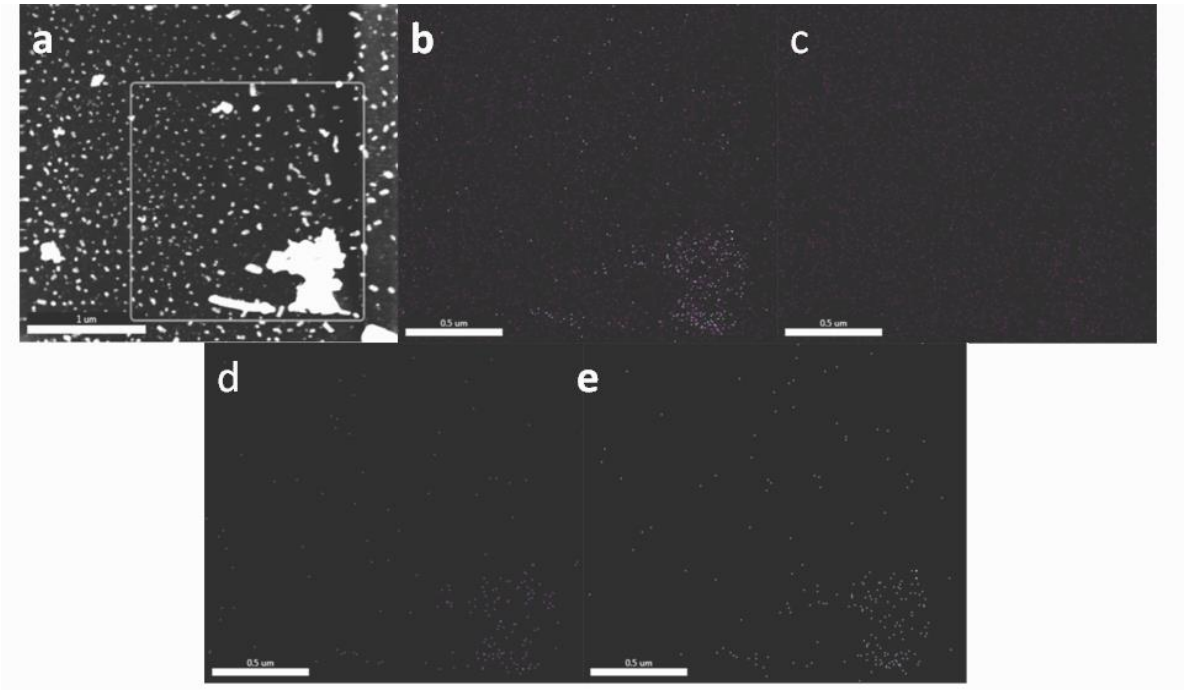

Figure 5.4 EDAX mapping of Pd@TTF a) STEM image Pd@TTF, Mapping of individual elements c) Carbon d) Sulphur e) Palladium.

5.3.3 Electro-activity of Pd@TTF

Figure 5.5 (A) shows the cyclic voltammograms of bare GC, GC/TTF and GC/Pd@TTF in 0.1M PBS (pH 7.4) solution. In case of bare GC no peak was observed and GC/TTF shows two oxidation peaks at 0.006 and 0.53V which is due to oxidation of TTF from TTF to TTF^{+} and TTF^{+} to TTF^{2+} respectively. In case of Pd@TTF almost 2.5 time increment in oxidation current was observed at both the oxidation peak position of TTF, which is due to the synergistic effect of Pd. Rastogi et al [Rastogi *et al.*, 1014] reported the oxidation of Pd in silica matrix at 0.55 V and reduction at -0.01 V, which is very close to the oxidation peaks of TTF and similar behaviour of Pd could also be expected in this case also that's why differential of oxidation peak of Pd from TTF peaks is very difficult.

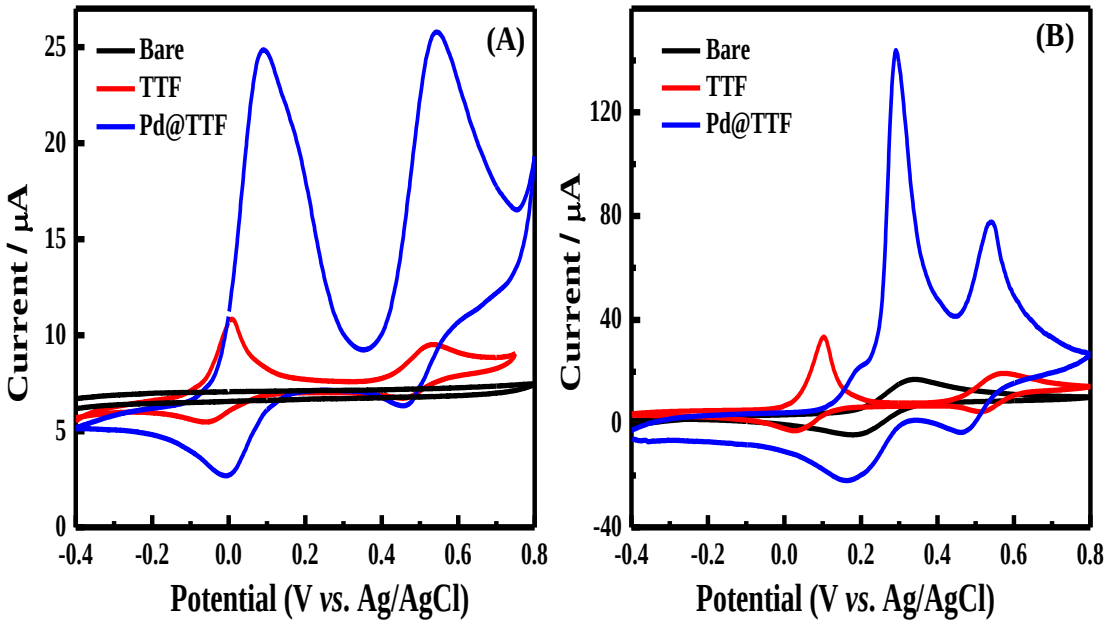

Figure 5.5 CVs of the electrodes (GC, GC/TTF and GC/Pd@TTF) in the absence (A) and presence of 5.0 mM of Fe (II)/Fe (III) redox couple (B) in 0.1 M phosphate buffer solution (pH 7.4).

Further, electrochemical behaviour of these electrodes (GC, GC/TTF and GC/Pd@TTF) was also studied in 5.0 mM of $Fe^{2+/3+}$ solution (pH 7.4) (Figure 5.5 B). In $Fe^{2+/3+}$ solution GC/TTF show 34 µA for TTF to TTF^{+} and 20 µA for TTF^{+} to TTF^{2+} conversion. Which have almost more than 2 times higher current as compared to GC/TTF in 0.1 M PBS only. Similarly GC/Pd@TTF shows tremendous increment in current (almost six times). Thus we have seen that, current observed for GC/Pd@TTF electrode is much higher as compared to GC/TTF which is due to synergistic effect Pd NPs. Further effective electrochemical surface area of bare GC and Pd@TTF/GCE electrodes were calculated using Randles -Sevick equation (1) [Bard *et al.*, 2000]

$$i_p = (2.69 \times 10^5)\, n^{3/2} A\, D^{1/2} C\, \upsilon^{1/2} \ldots\ldots\ldots\ldots\ldots (1)$$

Where, D is the diffusion constant (7.6×10^{-6} cm^2/s), C is the bulk concentration of $K_4[Fe(CN)_6]$ molar concentration, n is the no of electrons transferred, υ is the scan rate,

and A is the effective electrode surface area (EES). EES of bare, GC/TTF and GC/Pd@TTF electrodes were found to be was found to be 0.095, 0.101 and 0.178 cm^2 respectively. It has been observed that modified electrode shows quasi-reversible behaviour and there is an enhancement of current which can attribute to fast electron transfer kinetics and enhanced electro active surface area of modified electrode due to presence of Pd nanoparticles as shown in Figure 3B. However, an oxidation peak at 0.60 V could be due to oxidation of TTF radical cation.

5.3.4 Electro-catalytic Oxidation of CFZ

Figure 5.6.(A-C) shows the cyclic voltammograms of bare GC (A), GC/TTF (B) and GC/Pd@TTF (C) in absence (a) and presence (a') of 1.0 mM of CFZ. It was found that oxidation of CFZ at bare GC takes place around 1.0 V whereas at TTF and Pd@TTF modified electrodes oxidation occurs around 0.88V. Thus, oxidation of CFZ takes place around 120 mV less positive potential at TTF and Pd@TTF as compared to bare GC. Although oxidation of CFZ at TTF and Pd@TTF modified electrodes takes place approximately same potential but the oxidation current observed at Pd@TTF is much higher as compared to TTF, which is due to the synergistic effect of Pd nanoparticles.

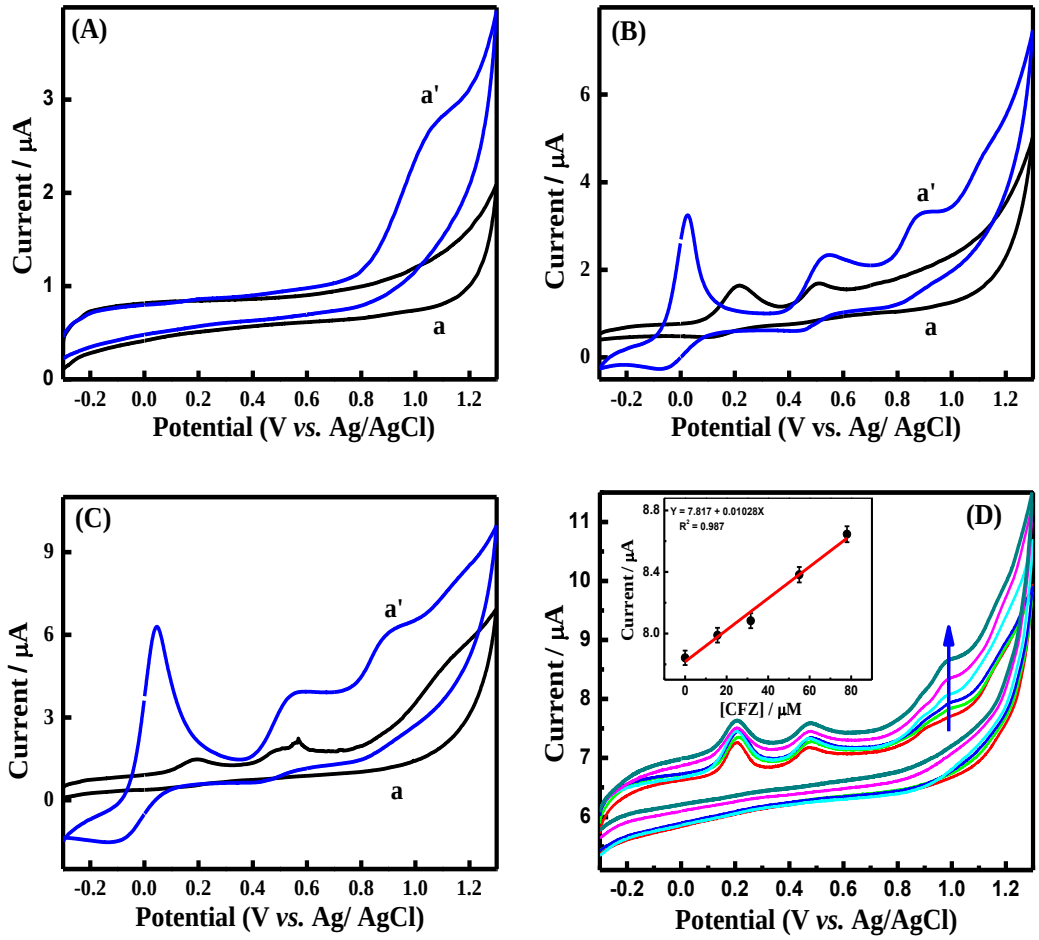

Figure 5.6 Cyclic voltammograms of bare GC (A), GC/TTF (B) and GC/Pd@TTF in absence (a) and presence of 1.0 mM of CFZ in 0.1 M PBS (pH 7.4) at scan rate 50 mVs^{-1}. (D) CV response of Pd@TTF after successive addition of CFZ (1.0, 15.0, 30.0, 55.0 and 78 µM). Insert shows the corresponding calibration plot.

Figure 5.6 D show the cyclic voltammograms of the GC/Pd@TTF with successive addition of CFZ. It was observed that the anodic current increases linearly with increasing concentration of CFZ (from 1.0 µM to 78 µM). Corresponding linear calibration plot is shown in inset of Figure 5.6 D. The prepared electrode shows linear behaviour from 1 µM to 78 µM with regression equation $I_{\mu A}$ = 7.817 + 0.01028 $[CFZ]_{\mu M}$. Till date, this is the broadest linear calibration range for CFZ determination by

electrochemical method. Detection limit and linear calibration of the proposed sensor together with previously published literature is tabulated in Table 5.1.

Table 5.1 Analytical parameters of the prepared electrode with other reported literature.

Electrode	**Techni--ques**	**Linear Calibration Range (µM)**	**Limit of detection (LOD) (µM)**	**References**
HME	DPV	0.1 - 0.15	0.0055	Ferreira *et al.*, 1997]
Ni/SDS/POAP/CPE	CPA	5-130	1.8	Fathi *et al.*, 2014
DME	LSV	10 - 100	-	Ferreira *et al.*, 1997
Poly L-lysine/HMDE	DPV	0.0007 - 0.00597	0.00011	Ferreira *et al.*, 1999
GC	DPV	4-80	0.6	Tarinc *et al.*, 2014
GC	SWV	4-20	1.0	Tarinc *et al.*, 2014
Pd-AuNPs-MWCNT/GCE	LSV	0.05 to 50	0.0001	Shahrokhian *et al.*, 2014
AgNPs-MIP/MWCNT/GCE	ASDPV	0.002 - 0.5	0.0055	Torkashvand *et al.*, 2016
Pd@TTF	CV	1.0 -78.0	0.5	Present work

DME = Dropping mercury electrode, MIP = Molecularly imprinted polymer, HME = Hanging mercury electrode. HMDE = Hanging mercury drop electrode

LSV = Linear sweep voltammetry, DPV = Differential pulse voltammetry, SWV = Square wave voltammetry, ASDPV = Anodic stripping differential pulse voltammetry.

From Table 5.1 it is clear that the analytical performance of the prepared electrode is comparable with previously reported literature.

As we have shown that, the oxidation of CFZ takes palace around at 0.88V along with two characteristic oxidation peaks of the Pd@TTF. On each successive addition of CFZ, oxidation peak current increases gradually and showed irreversible response due to oxidation of drug and forming by-products. Oxidation current increases probably due to the oxidation of aminothiazole moiety of CFZ *via* one electron transfer process [Blachin *et al.*, 1987; Ogorevc *et al.*, 1991]. Further, this molecule is dissociated due to instability of β-lactam ring into different by-products followed by isomerisation, lactonisation and epimerisation [Namiki *et al.*, 1987; Okamoto *et al.*, 1996].

5.3.5 Real Sample Analysis

The CFZ content in pharmaceutical formulations was in commercially available injection (250 mg CFZ) analyzed using the fabricated sensor in order to check its applicability. For this purpose, the required amount of the injection was taken and test solutions were prepared. CV measurements were performed under optimized parameters, and CFZ content was determined using calibration plot. The reported and calculated values of the CFZ content in respective pharmaceutical formulation are compared in Table 5.2. Further, solution was spiked with different amounts of standard CFZ, and the amounts of CFZ present in the mixtures were estimated. The results of the recovery (94 to 98 %) and RSD (2.3 to 3.4 %) showed that the present electrode can be

conveniently used for the determination of CFZ present in the pharmaceutical formulations.

Sample	**Amount of CEZ present in injection (mg)**	**Amount of standard CFZ spiked (mg)**	**Total amount present in the sample (mg)** (average of four measurements)	**Amount of CFZ found (mg)** (average of four measurements)	**Reco-very (%)**	**RSD (%) (n= 4)**
CFZ Injection	246	0	246	241.2	97.04	2.3
		10	256	248.1	96.9	3.1
		20	266	251.6	94.5	2.5
		30	276	269.5	97.6	3.4

Table 5.2 Determination of CFZ in pharmaceutical injection.

5.3.6 Stability and Reproducibility

Intraday stability of the prepared electrode was checked by measuring the current of the modified electrode before and after the experiment and approximately 2.5 %, loss in initial signal was observed after experiment. Inter-day stability and reproducibility was also checked by measuring the voltammetric signals obtained for 10 µM CFZ oxidation for 30 days. The current response showed a deviation of 5.7% for the first 15 days, however, after 15 days the voltammetric signal fluctuated by ~7.2 %. Thus, the results obtained showed that the fabricated sensor bears good stability and reproducibility.

5.4 Conclusions

In summary, facile and one-pot chemical synthesis route was employed for the synthesis of Pd@TTF without utilising any external reducing agent, stabiliser or any control of reaction parameter such as pH, temperature etc. Prepared Pd@TTF was characterized by using various techniques. TEM images reveal the spherical structure of Pd NPs and the average diameter of the prepared Pd NPs was found to be 30-40 nm. Prepared composite material shows efficient electrocatalytic activity for ceftazidime. Pd@TTF nanocomposite proved to be a highly efficient sensor for voltammetric determination of CFZ. The limit of detection (LOD) of CFZ was found to be 0.5 µM. The present method does not require any pre and post sample treatment. Prepared composite material can be used for the estimation of CFZ in pharmaceutical formulations.